Relativistic Descriptions of Final-State Interactions in Quasielastic Electron and Neutrino-Nucleus Scattering

C. Giusti, **A. Meucci**

Dipartimento di Fisica Nucleare e Teorica, Università degli Studi di Pavia and INFN, Sezione di Pavia, via Bassi 6 I-27100 Pavia, Italy

Abstract. Models developed within the framework of the relativistic impulse approximation for quasielastic (QE) electron and neutrino-nucleus scattering are discussed. Different descriptions of final-state interactions (FSI) in the inclusive scattering are compared: the relativistic Green's function (RGF) and the relativistic mean field (RMF). The results of the models are compared with the recently measured double-differential charged-current QE (CCQE) neutrino MiniBooNE cross sections.

1 Introduction

Several decades of experimental and theoretical work on electron scattering have provided a wealth of detailed information on nuclear structure and dynamics [1, 2]. Additional information is available from neutrino-nucleus scattering. Recently, muon charged-current (CC) neutrino-nucleus double differential cross sections have been measured by the MiniBooNE collaboration [3]. High-quality predictions for neutrino-nucleus cross sections are needed for use in ongoing experimental studies of neutrino oscillations at GeV energies and a proper analysis of data requires that the nuclear response to neutrino interactions is well under control and that the unavoidable uncertainties on nuclear effects are reduced as much as possible. Although the two situations are different, electron scattering is the best available guide to determine the predictive power of a nuclear model. Nonrelativistic and relativistic models have been used to describe nuclear effects with different approximations. Relativity is however important at all energies, in particular at high energies, and in the energy regime of many neutrino experiments a fully relativistic approach is required, where not only relativistic kinematics is considered, but also nuclear dynamics and current operators should be described within a relativistic framework.

Models for the QE exclusive and inclusive electron and neutrino scattering are presented in this contribution. In the QE region the nuclear response is dominated by the mechanism of one-nucleon knockout, where the probe interacts with a quasifree nucleon that is emitted from the nucleus with a direct one-step mechanism and the remaining nucleons are spectators. In the exclusive $(e, e'p)$

reaction the outgoing nucleon is detected in coincidence with the scattered electron, the residual nucleus is left in a specific discrete eigenstate and the final state is completely specified. In the inclusive (e, e') scattering only the scattered electron is detected, the final nuclear state is not determined, and the cross section includes all the available final nuclear states. The inclusive CC scattering where only the charged lepton is detected can be treated with the same models used for the inclusive (e, e') reaction.

For all these processes the cross section is obtained in the one-boson exchange approximation from the contraction between the lepton tensor, that under the assumption of the plane-wave approximation for the initial and the final lepton wave functions depends only on the lepton kinematics, and the hadron tensor $W^{\mu\nu}$, whose components are given by bilinear products of the matrix elements of the nuclear current J^μ between the initial and final nuclear states, *i.e.*,

$$W^{\mu\nu} = \sum_f \langle \Psi_f \mid J^\mu(\boldsymbol{q}) \mid \Psi_i \rangle \langle \Psi_i \mid J^{\nu\dagger}(\boldsymbol{q}) \mid \Psi_f \rangle \, \delta(E_i + \omega - E_f), \quad (1)$$

where ω and $\boldsymbol{q}$ are the energy and momentum transfer, respectively. Different but consistent models to calculate the components of the hadron tensor in QE electron and neutrino-nucleus scattering are outlined in the next sections.

2 The Exclusive $(e, e'p)$ Reaction

For the exclusive $(e, e'p)$ reaction a model based on the distorted-wave impulse approximation (DWIA) has been developed to calculate the matrix elements in Eq. (1). The model is based on the following assumptions [1, 2, 4]:

i) An exclusive process is considered, where the residual nucleus is left in a discrete eigenstate n of its Hamiltonian.

ii) The final nuclear state is projected onto the channel subspace spanned by the vectors corresponding to a nucleon, at a given position, and the residual nucleus in the state n. This assumption neglects effects of coupled channels and is justified by the considered asymptotic configuration of the final state.

iii) The (one-body) nuclear-current operator does not connect different channel subspaces and also the initial state is projected onto the selected channel subspace. This is the assumption of the direct-knockout mechanism and of the IA.

The amplitudes of Eq. (1) are then obtained in a one-body representation as

$$\lambda_n^{1/2} \langle \chi^{(-)} \mid j^\mu(\boldsymbol{q}) \mid \varphi_n \rangle, \quad (2)$$

where j^μ the one-body nuclear current, $\chi^{(-)}$ is the single-particle (s.p.) scattering state of the emitted nucleon, φ_n the overlap between the ground state of the target and the final state n, i.e., a s.p. bound state, and the spectroscopic factor λ_n is the norm of the overlap function, that gives the probability of removing from the target a nucleon leaving the residual nucleus in the state n. In the model the s.p. bound and scattering states are eigenfunctions of a non Hermitian energy dependent Feshbach-type optical potential and of its Hermitian

conjugate at different energies. In standard DWIA calculations phenomenological ingredients are usually employed: the scattering states are eigenfunctions of a phenomenological optical potential determined through a fit to elastic nucleon-nucleus scattering data and the s.p. bound states are obtained from mean-field potentials, or can be calculated in a phenomenological Woods-Saxon well.

The model can be formulated in a similar way within nonrelativistic [4] DWIA and relativistic RDWIA frameworks [5]. Both the DWIA and the RD-WIA have been quite successful in describing $(e, e'p)$ data in a wide range of nuclei and in different kinematics [2, 5–7].

3 Inclusive Lepton-Nucleus Scattering

In the inclusive scattering where only the outgoing lepton is detected all elastic and inelastic channels contribute and the complex potential, with imaginary terms designed to reproduce just the elastic channel, should be dismissed. Different approaches have been used to account for FSI. In the approaches based on the RDWIA, FSI have been accounted for by purely real potentials. The final nucleon state has been evaluated with the real part of the relativistic energy-dependent optical potential (rROP), or with the same relativistic mean field potential considered in describing the initial nucleon state (RMF) [8, 9]. However, the rROP is unsatisfactory from a theoretical point of view, since it is an energy-dependent potential, reflecting the different contribution of open inelastic channels for each energy, and under such conditions dispersion relations dictate that the potential should have a nonzero imaginary term [10]. On the other hand, the RMF model is based on the use of the same potential for bound and scattering states. It fulfills the dispersion relations [10] and also the continuity equation.

A different description of FSI makes use of Green's function (GF) techniques [11–17]. In the GF model, under suitable approximations that are basically related to the IA, the components of the hadron tensor are written in terms of the s.p. optical model Green's function. This result has been derived by arguments based on multiple scattering theory [10] or by means of projection operators techniques within nonrelativistic [11] and relativistic [12–14] frameworks. The explicit calculation of the s.p. Green's function can be avoided [11–13] by its spectral representation, that is based on a biorthogonal expansion in terms of a non Hermitian optical potential $\mathcal{H}$ and of its Hermitian conjugate $\mathcal{H}^{\dagger}$. Calculations require matrix elements of the same type as the DWIA ones in Eq. (2), but involve eigenfunctions of both $\mathcal{H}$ and $\mathcal{H}^{\dagger}$, where the imaginary part gives in one case absorption and in the other case gain of flux, and in the sum over n the total flux is redistributed and conserved. The GF model allows to recover the contribution of non-elastic channels starting from the complex optical potential that describes elastic nucleon-nucleus scattering data. It provides a consistent treatment of FSI in the exclusive and in the inclusive scattering and gives also a good description of (e, e') data [11, 12, 18].

For the inclusive electron scattering both nonrelativistic GF [11, 15] and rel-

ativistic RGF [12] models have been considered, for CC neutrino scattering the RGF model has been adopted [13]. The results of the RMF and RGF models have been compared in [18] for the inclusive electron scattering and in [20] for the inclusive CC neutrino scattering. An example is shown in Figure 1, where the RGF, RMF, and rROP cross sections of the ^{12}C(e, e') reaction calculated in a kinematics with a fixed value of the incident electron energy ($\varepsilon = 1$ GeV), and two values of the momentum transfer ($q = 500$ and 1000 MeV/c) are displayed. Two parameterizations of the ROP have been used for the RGF calculations, *i.e.*, the energy-dependent and A-dependent EDAD1 (RGF1) and EDAD2 (RGF2) [19]. The results of the relativistic plane-wave IA (RPWIA), where FSI are neglected, are also shown in the figure.

The differences between the RMF and RGF results, as well as the differences between RGF1 and RGF2, increase with the momentum transfer. At q = 500 MeV/c the three results are similar, both in magnitude and shape, larger differences are obtained at $q = 1000$ MeV/c. The shape of the RMF cross section shows an asymmetry, with a tail extending towards higher values of ω, that is essentially due to the strong energy-independent scalar and vector potentials present in the RMF model. The asymmetry towards higher ω is less significant but still visible for RGF1 and RGF2, whose cross sections show a similar shape but a significant difference in magnitude. At $q = 1000$ MeV/c both the RGF1 and RGF2 cross sections are higher than the RMF one in the maximum region, but a stronger enhancement is obtained with RGF1, which at the peak overshoots the RMF cross section up to 40% and it is even higher than the RPWIA result.

The differences between the RGF1 and RGF2 results are consistent with the general behavior of the two ROP's and are basically due to their imaginary part. The real terms are very similar and the rROP cross sections are not sensitive to the parameterization considered. The scalar and vector components of the real part of the ROP get smaller with increasing energies and the rROP result approaches the RPWIA one for large values of ω. In contrast, the imaginary part presents its maximum strength around 500 MeV, being also sensitive to the particular ROP parameterization.

An example for the ^{12}C (ν_μ, μ^-) cross section is shown in Figure 2. For the RGF model, the RGF1 results are compared with the results obtained with the energy-dependent but A-independent EDAI potential (RGF-EDAI). Calculations have been carried out with the same incident lepton energy and momentum transfer as for the (e, e') cross sections of Figure 1. Also in Figure 2 the shape of the RMF cross section shows an asymmetry with a tail extending towards higher values of ω (corresponding to lower values of the kinetic energy of the outgoing muon T_μ). An asymmetric shape is shown also by the RGF cross sections, while no visible asymmetry is given by the RPWIA and rROP results. Also in this case the differences between the RGF and rROP cross sections are consistent with the general behavior of the ROP's and are due to their different imaginary part. As already shown for the (e, e') reaction, the RGF yields in general a larger cross section than the RMF. This may reflect the influence of the pionic degrees of
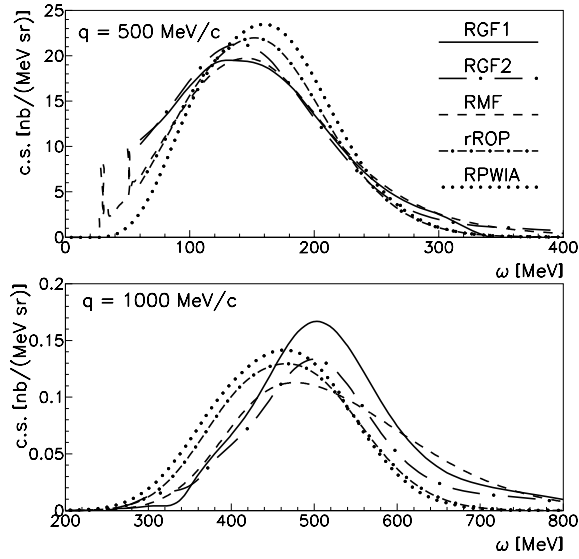
Figure 1. Differential cross section of the $^{12}C(e, e')$ reaction for an incident electron energy $\varepsilon = 1$ GeV and $q = 500$ and 1000 MeV/c. Results for RPWIA (dotted), rROP (dot-dashed), RGF1 (solid), RGF2 (long dot-dashed), and RMF (dashed) are compared.
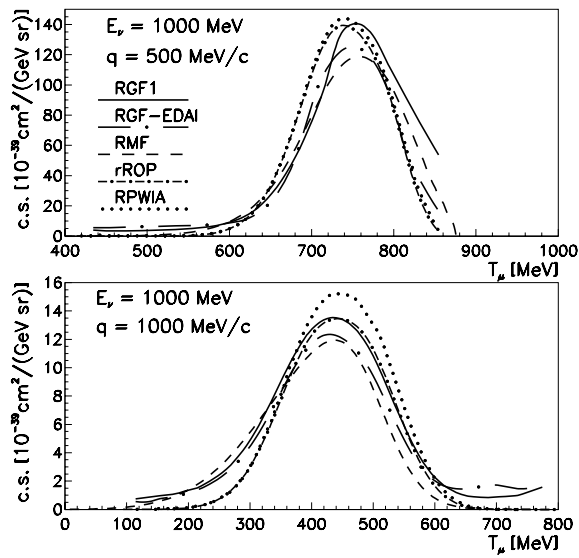

Figure 2. Differential cross section of the $^{12}C(\nu_\mu, \mu^-)$ reaction for $E_\nu = 1000$ MeV and $q = 500$ MeV/c and 1000 MeV/c. Results for RPWIA (dotted), rROP (dot-dashed) RGF1 (solid), RGF- EDAI (long dot-dashed), and RMF (dashed) are compared.

freedom, that can be included in a phenomenological way in the imaginary part of the ROP [18, 20].

The results in Figure 2 present some differences with respect to the corresponding (e, e') cross sections in Figure 1. In both cases the differences between the results of the different models are generally larger for increasing value of the momentum transfer. For neutrino scattering, however, such a behavior is less evident and clear. In particular, the RGF1 cross section at $q = 1000$ Mev/c does not show the strong enhancement in the region of the maximum shown in Figure 1, where the RGF1 result is even larger than the RPWIA one. In the case of neutrino scattering the RGF results in the region of the maximum are generally larger than the RMF ones, but smaller than the RPWIA cross sections. The numerical differences between the RGF results for electron and neutrino scattering can mainly be ascribed to the combined effects of the weak current, in particular its axial term, and the imaginary part of the ROP [20].

4 Scaling Functions

The comparison has been extended to the scaling properties of the different models [18, 20]. Scaling ideas applied to inclusive QE electron-nucleus scattering have been shown to work properly to high accuracy [22, 23]. At sufficiently high momentum transfer a scaling function is derived dividing the experimental (e, e') cross sections by an appropriate single-nucleon cross section. This is basically the idea of the IA. If this scaling function depends only upon one kinematical variable, the scaling variable, one has scaling of first kind. If the scaling function is roughly the same for all nuclei, one has scaling of second kind. When both kinds of scaling are fulfilled, one says that superscaling occurs. An extensive analysis of electron scattering data has shown that scaling of first kind is fulfilled at the left of the QE peak and broken at its right, whereas scaling of second kind is well satisfied at the left of the peak and not so badly violated at its right. A phenomenological scaling function $f_L^{exp}(\psi')$ has been extracted from data of the longitudinal response in the QE region. The dimensioneless scaling variable $\psi'(q, \omega)$ is extracted from the relativistic Fermi gas (RFG) analysis that incorporates the typical momentum scale for the selected nucleus [9, 22]. Although many models based on the IA exhibit superscaling, only a few of them are able to reproduce the asymmetric shape of $f_L^{exp}(\psi')$ with a significant tail extended to high values of ω (large positive values of ψ'). One of these is the RMF model. In contrast, the RPWIA and the rROP lead to symmetrical-shape scaling functions which are not in accordance with data analysis [9, 21]. The scaling function of the RGF and RMF are very similar for lower values of the momentum transfer ($q = 500 - 700$ MeV/c) and in good agreement with the phenomenological function [18], the asymmetric tail of the data and the strength at the peak are fairly reproduced by both models, while visible discrepancies appear increasing q.

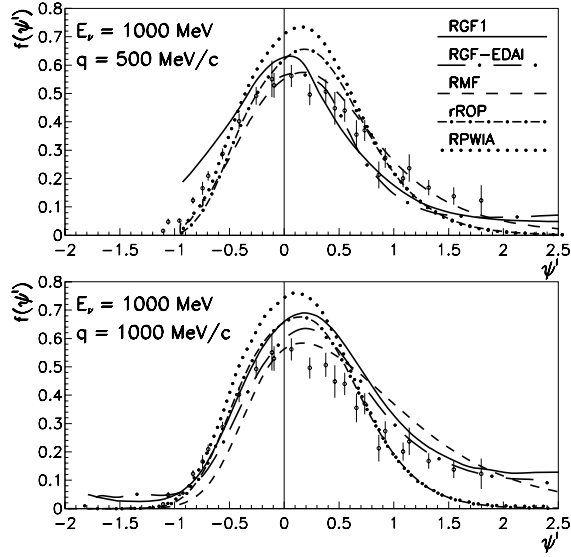In Figure 3 the scaling function extracted from the differential cross sections

Figure 3. Scaling function of the ^{12}C(ν_μ, μ^-) reaction for incident neutrino energy E$_\nu$ = 1000 MeV and q = 500 MeV/c and 1000 MeV/c. Line convention as in Figure 2

of the ^{12}C(ν_μ, μ^-) reaction evaluated for different models at q = 500 and 1000 MeV/c (shown in Figure 2) are compared with the phenomenological scaling function extracted from the analysis of (e, e') data. Both the RMF and the RGF models give an asymmetric shape, with a tail in the region of positive ψ'. In contrast, the RPWIA and the rROP results do not show any significant asymmetry. As a general remark, these results for the scaling functions follow similar trends to those already applied to the behavior of the cross sections in Figure 2.

5   Comparison with Charged-Current Quasielastic MiniBooNE data

The CCQE ^{12}C(ν_μ, μ^-) cross sections recently measured by the MiniBooNE collaboration [3] have raised debate over the role of the theoretical ingredients entering the description of the reaction. The experimental cross section is underestimated by the RFG model, and by other more sophisticated models, unless the nucleon axial mass M_A is significantly enlarged (1.35 GeV/c^2 in the RFG) with respect to the accepted world average value (1.03 GeV/c^2 [24, 25]). Before drawing conclusions about the value of the axial mass it is however important to evaluate carefully the contributions of all the nuclear effects. Within the QE kinematic domain the treatment of FSI is essential for the comparison with data. The comparison between the results of the RMF and RGF models can be helpful for a deeper understanding of the role played by FSI in the analysis of CCQE data [26].

The CCQE double-differential ^{12}C (ν_μ, μ^-) cross sections averaged over

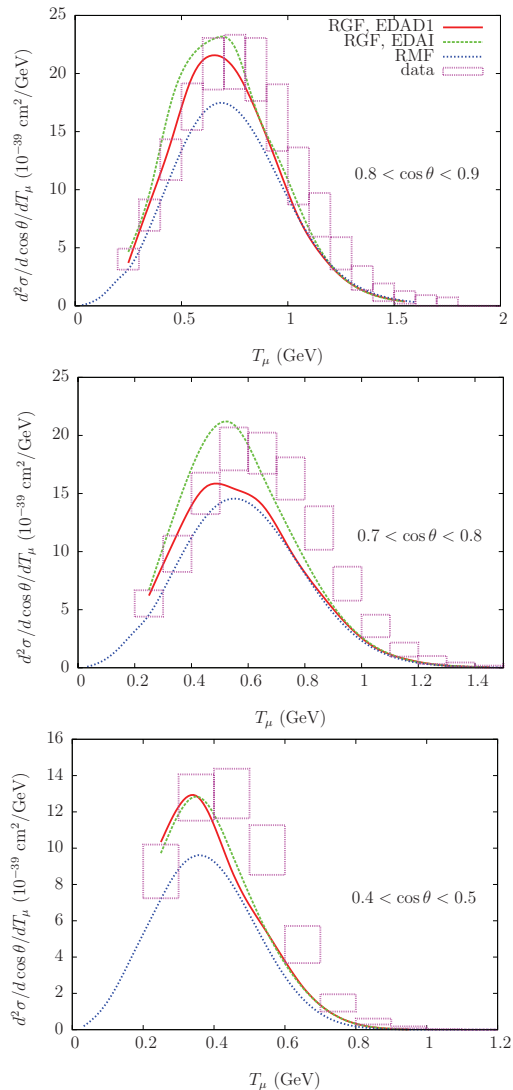Figure 4. Flux-averaged double-differential cross section per target nucleon for the CCQE ^{12}C(ν_μ, μ^-) reaction calculated in the RMF (blue line), the RGF1 (red), and RGF-EDAI (green) and displayed versus T_μ for various bins of $\cos\theta$. In all the calculations the standard value of the nucleon axial mass, *i.e.*, $M_A = 1.03$ GeV/c^2 has been used. The data are from MiniBooNE [3].

the neutrino flux as a function of T_μ for various bins of $\cos\theta$, where θ is the muon scattering angle, are shown in Figure 4. The RMF results yield reasonable agreement with data for small angles and low muon energies, the discrepancy

becoming larger as θ and T_μ increase. The shape followed by the RMF and RGF cross sections fits well the slope shown by the data. The two models yield close predictions at larger values of T_μ, for all the bins of $\cos\theta$ shown in the figure. The RGF cross sections are generally larger than the RMF ones. The differences increase approaching the peak region, where the additional strength shown by the RGF produces cross sections in reasonable agreement with the data. The differences between the RGF-EDAI and RGF-EDAD1 results are enhanced in the peak region and are in general of the order of the experimental errors.

In Figure 5 the total CCQE cross section per neutron obtained in the RMF and RGF models are displayed as a function of the neutrino energy and compared with the "unfolded" experimental data [3]. The RMF results underpredict the MiniBoone cross section. Larger cross sections, in particular for larger values of E_ν, are obtained in the RGF with both optical potentials. Visible differences are obtained between the RGF-EDAI and the RGF-EDAD1 results, being RGF-EDAI in good agreement with the shape and magnitude of the experimental cross section and RGF-EDAD1 above RMF but clearly below the data. These differences are due to the different imaginary parts of the two ROP's, particularly for the energies considered in kinematics with the lowest θ and the largest T_μ. These kinematics, which were not considered in previous calculations [13, 20], give large contributions to the total cross section and emphasize the differences between the RGF predictions with the two optical potentials. We notice that EDAI is a single-nucleus parameterization, which does have an edge in terms of better reproduction of the elastic proton-^{12}C phenomenology [19] compared to EDAD1, and also leads to CCQE results in better agreement with data.

The RMF model generally underpredicts the data [27]. In contrast, the RGF can give cross sections of the same magnitude as the experimental ones without
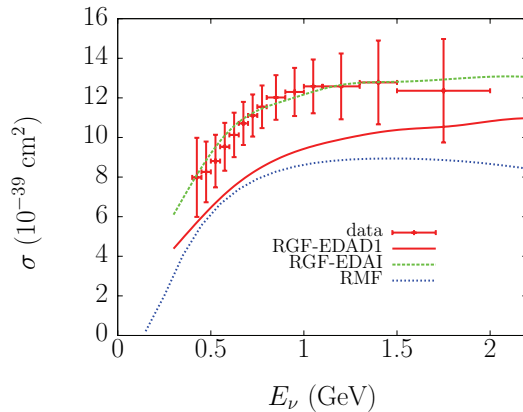

Figure 5. Total CCQE cross section per neutron versus the neutrino energy. The cross sections calculated in the RMF (blue line), RGF EDAD1 (red), and RGF EDAI (green) potentials are compared with the flux unfolded MiniBooNE data of [3].

the need to increase the standard value of the axial mass. The larger cross sections arise in the RGF model from the translation to the inclusive strength of the overall effect of inelastic channels.

These results confirm that before drawing conclusions about the comparison with CCQE MiniBoone data and the need to increase the axial mass, the relevance of all nuclear effects must be investigated. A careful evaluations of the relevance of multi-nucleon emission [28, 29] and of some non-nucleonic contributions [30] would be helpful to clarify the content of the enhancement of the CCQE cross sections obtained in the RGF model. A better determination of a phenomenological ROP which closely fullfills the dispersion relations deserves further investigation.

Acknowledgements

References

[1] S. Boffi, C. Giusti, F.D. Pacati, *Phys. Rep.* **226** (1993) 1-101.

[2] S. Boffi, C. Giusti, F.D. Pacati, M. Radici, *Electromagnetic Response of Atomic Nuclei* Oxford Studies in Nuclear Physics, Vol. 20, Clarendon Press, Oxford (1996).

[3] A.A. Aguilar-Arevalo *et al.*, *Phys. Rev.D* **81** (2010) 092005-1-22.

[4] S. Boffi, F. Cannata, F. Capuzzi, C. Giusti, F.D. Pacati, *Nucl. Phys. A* **379** (1982) 509-522.

[5] A. Meucci, C. Giusti, F.D. Pacati, *Phys. Rev. C* **64** (2001) 014604-1-10.

[6] J.M. Udías, P. Sarriguren, E. Moya de Guerra, E. Garrido, J.A. Caballero, *Phys. Rev. C* **48** (1993) 2731-2739.

[7] M. Radici, A. Meucci, W.H. Dickhoff, *Eur. Phys. J. A* **17** (2003) 65-69.

[8] C. Maieron, M.C. Martínez, J.A. Caballero, J.M. Udías, *Phys. Rev. C* **68** (2003) 048501-1-4.

[9] J.A. Caballero, *Phys. Rev. C* **74** (2006) 015502-1-12.

[10] Y. Horikawa, F. Lenz, N.C. Mukhopadhyay, *Phys. Rev. C* **22** (1980) 1680-1695.

[11] F. Capuzzi, C. Giusti, F.D. Pacati *Nucl. Phys.A* **524** (1991) 681-705

[12] A. Meucci, F. Capuzzi, C. Giusti, F.D. Pacati, *Phys. Rev.C* **67** (2003) 054601-1-12.

[13] A. Meucci, C. Giusti, F.D. Pacati *Nucl. Phys. A* **739** (2004) 277-290.

[14] A. Meucci, C. Giusti, F.D. Pacati *Nucl. Phys. A* **756** (2005) 359-381.

[15] F. Capuzzi, C. Giusti, F.D. Pacati, D.N. Kadrev, *Ann. Phys.* **317** (2005) 492-529.

[16] A. Meucci, C. Giusti, F.D. Pacati, *Acta Phys. Polon. B* **37** (2006) 2279-2286.

[17] A. Meucci, C. Giusti, F.D. Pacati, *Acta Phys. Polon. B* **40** (2009) 2579-2584.

[18] A. Meucci, J.A. Caballero, C. Giusti, F.D. Pacati, J.M. Udías, *Phys. Rev. C* **80** (2009) 024605-1-12.

[19] E.D. Cooper, S. Hama, B.C. Clark, R.L. Mercer, *Phys. Rev. C* **47** (1993) 297-311.

[20] A. Meucci, J.A. Caballero, C. Giusti, F.D. Pacati, and J.M. Udías, *Phys. Rev. C* **83** (2011) 064614-1-10.

[21] J.A. Caballero, J E Amaro, M.B. Barbaro, T.W. Donnelly, C. Maieron, J.M. Udías, *Phys. Rev. Lett.* **95** (2005) 252502-1-4.

[22] C. Maieron, T.W. Donnelly, and I. Sick, *Phys. Rev. C* **65** (2002) 025502-1-15.

[23] T.W. Donnelly and I. Sick, *Phys. Rev. Lett.* **82** (1999) 3212-3215;
— — *Phys. Rev. C* **60** (1999) 065502-1-16.

[24] V. Bernard, L. Elouadrhiri and U.G. Meissner, *J. Phys.G* **28** (2002) R1-R35.

[25] A. Bodek, S. Avvakumov, R. Bradford, H. Budd, *Eur. Phys. J. C* **53** (2008) 349-354.

[26] A. Meucci, M.B. Barbaro, J.A. Caballero, C. Giusti C, J.M. Udías, *Phys. Rev. Lett.* **107** (2011) 172501-1-5.

[27] J.E. Amaro, M.B. Barbaro, J.A. Caballero, T.W. Donnelly, J.M. Udías, *Phys.Rev. D* **84** (2011) 033004-1-8.

[28] M. Martini, M. Ericson, G. Chanfray, J.Marteau, *Phys. Rev. C* **80** (2009) 065501-1-16;
— — *Phys. Rev. C* **81** (2010) 045502-1-5.

[29] J. Nieves, I. Ruiz Simo, M.J. Vicente Vacas, *Phys. Rev. C* **83** (2011) 045501-1-19;
— — *Preprint arXiv:1106.5374 [nucl-th]* (2011).

[30] T. Leitner, U. Mosel, *Phys. Rev. C* **81** (2010) 064614-1-10.